SCIENCE CHINA
Technological Sciences

•Article•

June 2018 Vol.61 No.6: 916–922
https://doi.org/10.1007/s11431-017-9231-1

Experimental study of heat-transfer coefficient of Al-Zn-Mg-Cu ultra-thick hot plate during multi-stage quenching

FAN ShiTong[1], DENG YunLai[1,2], ZHANG Yong[1*], HUANG XinYue[1] & WU PengFei[1]

[1]*School of Materials Science and Engineering, Central South University, Changsha 410083, China;*
[2]*State Key Laboratory of High Performance and Complex Manufacturing, Central South University, Changsha 410083, China*

Received February 7, 2017; accepted March 14, 2018; published online April 24, 2018

Experiments were conducted to investigate the cooling manner of an ultra-thick hot aluminum alloy plate during multistage quenching. Cooling curves and heat flux curves of different rapid quenching flux varied from 23 to 40 L min^{-1} and were analyzed in detail. In this investigation, cooling process was divided into the following four steps: (I) starting step, (II) rapid cooling step, (III) slow cooling step, and (IV) stopping step. Based on the curves, the calculation method for surface transfer coefficient was provided, and the effects of coefficient on surface temperature and quenching flux were discussed. Results showed that the transfer coefficient disagreed with heat flux and that it is a nonlinear function of surface temperature. The highest coefficient was observed not in the rapid cooling step with the largest heat flux but in the slow cooling step with lower heat flux. The coefficient increased with surface temperature ranging from 480 to 150°C, and a coefficient peak appeared in the temperature range of 150–100°C. The coefficient also increased with quenching flux. Finally, a simulation was performed using the finite element method to verify the reliability of the coefficient results, which showed good agreement with the measurement values.

heat transfer coefficient, multi-stage quenching, aluminum alloy, plate, finite element method

Citation: Fan S T, Deng Y L, Zhang Y, et al. Experimental study of heat-transfer coefficient of Al-Zn-Mg-Cu ultra-thick hot plate during multi-stage quenching. Sci China Tech Sci, 2018, 61: 916–922, https://doi.org/10.1007/s11431-017-9231-1

1 Introduction

Al-Zn-Mg-Cu aluminum alloys are developed to satisfy aviation demands. With the development of design ideas in integral component manufacturing, the demand for large-sized and high-performance aluminum alloy increases significantly in the aviation industry [1]. A larger and more integral structure avoids traditional welding and riveting; this advantage can raise reliability and reduce weight. However, integral component manufacturing calls for strict requirements in size, comprehensive properties, and homogeneity [2]. In the thickness direction, performance homogeneity, such as inhomogeneity in heat treatment structures and residual stress, is the key to designing and manufacturing aluminum plates. After quenching, at the center layer of the plate, inhomogeneity precipitation of the equilibrium phase at the grain and phase boundaries would lead to low comprehensive performance because of insufficient strengthening of precipitates during aging. The residual stress generated in quenching is extremely high to be eliminated by pre-stretching [3,4]. Inhomogeneity and residual stress have been considered important challenges for international aluminum processing industry [5–7].

Inhomogeneity of mechanical properties and residual stress are both related directly and inversely, respectively, to the cooling rate of the plate. With increasing thickness, the cooling rate of the center reduces and the temperature difference between the surface and center increases, resulting in slack quenching in the center and high residual stress, respectively. To improve the mechanical properties, the cool-

* Corresponding author (email: yongzhang2017@163.com)

ing rate must be increased. However, the cooling rate must be reduced to decrease the residual stress. Hence, a proper cooling rate should coordinate the mechanical properties of the center and residual stress, and temperature field prediction initially solves this problem.

Heat transfer in plate quenching includes convection with water, radiation, and center-to-surface conduction. Convection and radiation can be summarized to describe surface heat transfer, whereas conduction is based on the decrease in surface temperature. Therefore, to predict the temperature field, surface heat transfer coefficient must be calculated precisely. Aiming at the surface heat transfer coefficient of the plate, numerous research has been performed on the subject of steel with the inverse method [8–10]. Price and Fletcher [11] studied the effects of the surface temperature on the surface heat transfer coefficient of steel in water, polymer, and oil quenchants. They observed the association of the cooling effect with the degree of stability of the vapor blanket produced during the early stages of quenching.

However, only several investigations focused on aluminum plates [12,13]. Wang et al. [14] studied heat transfer on a hot plate during water jet impingement cooling and observed that the surface temperature significantly influenced the coefficient. Zhang et al. [15] designed a multistage quenching process for a 7050 aluminum alloy to increase the heat-transfer coefficient, reduce the residual stress, and obtain the coefficient via the end-quenching method. Sample size is extremely small to reflect the industrial practices. Other researchers have directly studied quenching properties and residual stress [16–18], thus avoiding the influence of the cooling step. Hence, little attention has been paid to the cooling mechanism of industrial scale aluminum plates.

In the present investigation, an industrial scale ultra-thick aluminum plate was used to study the cooling mechanism in a roller-type spray quenching furnace. A heat preventing facility was designed to measure the real-time temperature. Based on the actual cooling curve, the surface transfer coefficient of the aluminum plate and the calculation method were studied. The coefficient was finally verified via the finite element method.

2 Materials and methods

2.1 Material and experimental facilities

An aluminum alloy ultra-thickness plate with a nominal composition of Al-2.2Cu-2.0Mg-6.5Zn-0.12Zr-0.05Ti (wt. %) was selected for investigation. Plate size spanned 180 mm (ND)×1100 mm (TD)×1300 (RD) mm. Table 1 shows the thermal properties of the alloy from 20 to 500°C; the density was considered to be constant.

Figure 1 illustrates the experimental facility. Heat transfers of the upper and lower surfaces were considered to be the same. Thus, the thermocouples were only set in the upper part of the plate. To set the thermocouples, a 10-mm deep groove was first milled in the upper part of the plate. Then, four holes with a size of Φ8×90 (depth) mm were drilled with thicknesses of 5, 30, 60, and 90 mm in the normal direction (see Figure 1). After mounting the thermocouples in the holes, asbestos was plugged into the holes to prevent water from entering and to direct heat transfer to the thermocouples. Outside the holes, high temperature adhesive was used to immobilize the thermocouples to ensure the direct contact between the material and these devices. Finally, massive asbestos was plugged into the groove and was immobilized by a steel sheet to achieve better waterproof and heat prevention.

A thermos detector is a real-time and heat-resistant temperature measuring facility. In the present study, the measurement interval was 0.2 s. The facility was placed on the other aluminum sheet connected to the temperature-measuring plate. The thermos-detector was also wrapped with asbestos to prevent heat transfer and was placed in a steel protector to prevent water from entering.

The thermocouple in the first hole (5 mm) was connected with the upper face of the hole. The distance from the upper surface to thermocouple reached 1 mm. As the surface temperature cannot be measured directly, the temperature

Table 1 Thermal properties of the plate

Temperature (°C)	Conductivity (W m^{-2} °C^{-1})	Specific heat (J kg^{-1} °C^{-1})	Density (kg m^{-3})
20	1.45×10^{2}	8.37×10^{2}	2850
100	1.50×10^{2}	8.96×10^{2}	
200	1.55×10^{2}	9.63×10^{2}	
300	1.60×10^{2}	1.05×10^{3}	
400	1.65×10^{2}	1.13×10^{3}	
500	1.70×10^{2}	1.19×10^{3}	

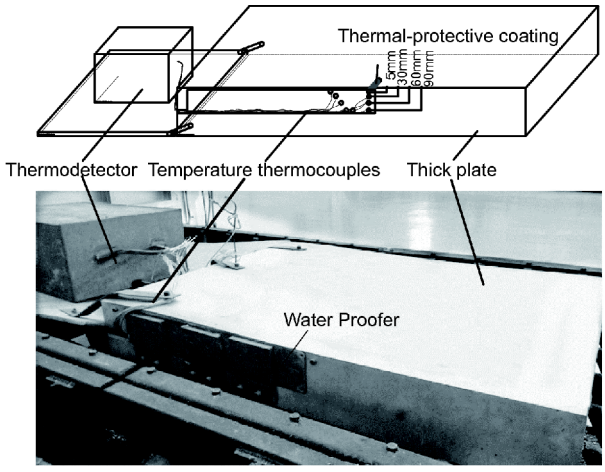

Figure 1 Sketch of the experimental facility.

measured in the first hole was considered as the surface temperature of the plate.

2.2 Experimental procedures

Figure 2 shows the experimental procedure. The plate was first heated to 480°C in the solution furnace. Then, it moved sequentially from the entrance area to the large flow area and small flow area and finally settled in the small flow area. The moving speed was 100 mm s^{-1}, and the time to leave the areas reached 6, 42, and 78 s. Total measurement time was 150 s. The plate was maintained from 78 to 150 s in the small flow area. In this experiment, the flux of the small flow area remained unchanged, while the effect of flux of the large flow area on heat transfer coefficient was studied. Table 2 shows the testing technology.

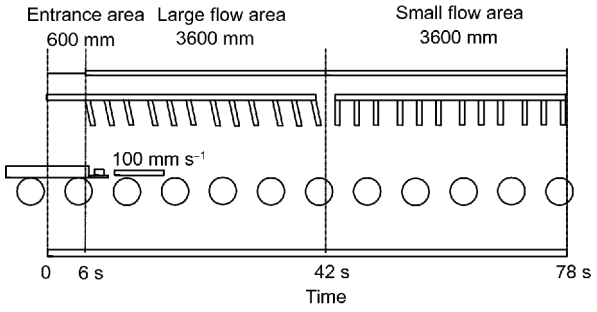

Figure 2 Sketch of the experimental procedure.

3 Results and discussion

3.1 Cooling curves and heat flux curve

Figure 3 displays the cooling curves in different thicknesses of various flux. As the temperature at different thicknesses is known, heat flux at every second can be calculated. As stated above, heat transfers of the upper and lower surfaces were assumed to be the same, and only the upper half of the plate was considered. Within $t-\Delta t$ to t seconds, the heat flux taken away by water flow equals heat reduction (φ) of the plate, and it can be calculated as a function of decrease in temperature as follows:

$$\varphi = c_p \rho A \int_0^{l/2} (T_{t-\Delta t} - T_t) \mathrm{d}l, \quad (1)$$

Table 2 Testing processes

Test Number	Flux of large flow area (L min^{-1})	Flux of small flow area (L min^{-1})	Moving speed (m s^{-1})
L40	40		
L35	35	23	0.1
L23	23		

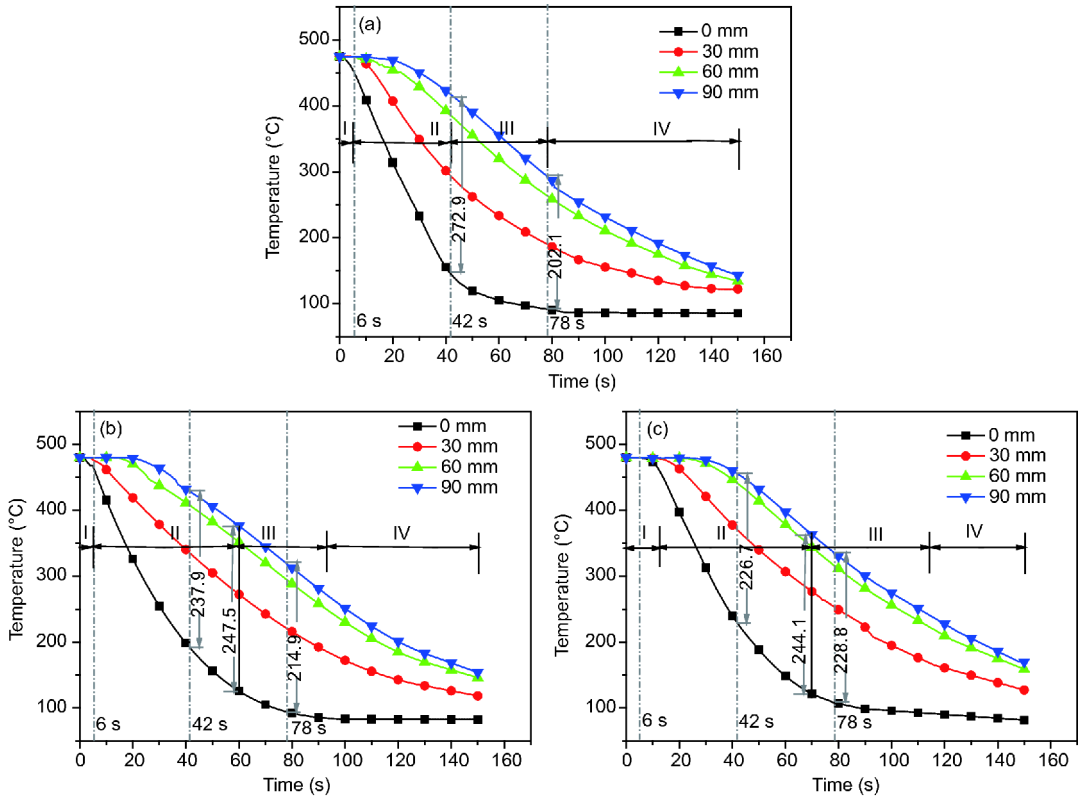

Figure 3 (Color online) Cooling curves in different thicknesses of various flux, cooling processing can be divided into the following four steps: (I) starting step, (II) rapid cooling step, (III) slow cooling step, and (IV) stopping step. Flux of the large flow area measured (a) 40, (b) 35, and (c) 23 L min^{-1}.

where c_p refers to the specific thermal capacity of the plate; ρ represents the density; A is the upper surface area; T_t and $T_t-\Delta t$ are temperature fields of t and $t-\Delta t$ moment, respectively; l corresponds to the plate thickness.

Figure 4 shows the heat flux curves calculated by eq. (1) in every second of different quenching flux. Comparing the cooling curves (Figure 3) and heat flux curves (Figure 4), similar cooling trends were observed for different quenching flux. Based on the curves and considering the cooling areas passed by the plate in the quenching furnace (see Figure 2), cooling process can be divided into the following four steps: starting step, rapid cooling step, slow cooling step, and stopping step.

(I) Starting step: When the plate was removed from the solution furnace and transferred into the entrance area, owing to the absence of water flow, the cooling rate was remarkably slow, and this very slow cooling step was defined as the starting step. When the flux of the large flow area reached 40 and 35 L min^{-1}, the duration of the starting step totaled 6 s, which was the time required by the plate to pass through the entrance area. However, when the flux totaled 23 L min^{-1}, the length was 11 s, and the plate had already moved into the large flow area. At the beginning of the cooling process, a considerable amount of water was evaporated. Then, the plate was surrounded by plenty of vapor, which prevented heat transformation. When the quenching flux was sufficiently large, the vapor would be pushed away by water jet impingement, thus resulting in a minimal influence on test L40 and L35. However, in L23, the cooling effect was prevented by vapor, and the duration of the starting step was prolonged.

(II) Rapid cooling step: In rapid cooling step, the surface cooling rate peaked immediately. Surface temperature decreased significantly, and the cooling rate changed minimally and remained at a high value. However, in the interior layer, the cooling rate was initially slow, but it accelerated gradually because of the increasing temperature difference between the surface and the interior. When the interior cooling rate reached that of the surface, the temperature was the highest, and the step was concluded at this moment.

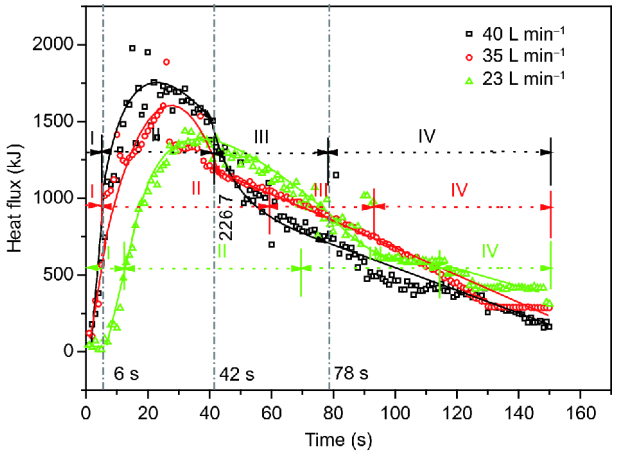

Figure 4 (Color online) Heat flux curves of different quenching flux, cooling process can be divided into the following four steps: (I) starting step, (II) rapid cooling step, (III) slow cooling step, and (IV) stopping step.

As shown in Figure 3, maximum temperature differences between the surface and the center of test L40, L35, and L23 reached 272.9, 247.5, and 244.1°C, whereas the moments spanned 42, 60, and 70 s, respectively. Results indicated that the rapid cooling step not only occurred in the large flow area. With the decrease in quenching flux, the length of this step was also prolonged. Corresponding to the cooling curves, heat flux (see Figure 4) of the three tests reached a significantly high level of over 1000 kJ in every second throughout the step. In this step, heat flux peaks decreased with decreasing quenching flux, and the peak time was also delayed.

(III) Slow cooling step: When the cooling rate at the surface was lower than that of the center, the slow cooling step started. In this step, the surface temperature was low, and the temperature difference between surface and surrounding decreased significantly. Thus, the surface cooling rate decreased. However, the center cooling rate, depending on surface temperature, remained at high levels because of the large temperature difference. Heat flux also decreased remarkably, as shown in Figure 4.

(IV) Stopping step: No clear distinction was observed between the stopping step and the slow cooling step. In this step, the surface temperature changed minimally, and the heat flux decreased with time.

Notably, for aluminum quenching, the most critical step is the rapid cooling step. In this step, the temperature difference between surface and center reached its peak, corresponding strongly with the mechanical properties and residual stress of the plate. As shown in Figure 3, the surface of the plate cooled down first, and the center was cooled by heat conduction depending on temperature difference. Thus, the center cooling rate was significantly high with a large temperature difference, thus leading to improved mechanical properties. However, the large temperature difference will cause high compressive residual stress in the surface layer and tensile stress in the center. Hence, controlling the cooling rate of the rapid cooling step is the key to coordinating the mechanical properties and resident stress. The cooling rate can also be predicted based on the heat transfer coefficient.

3.2 Effect on heat-transfer coefficient

3.2.1 Calculation of heat-transfer coefficient

As stated above, the half plate was used to calculate the heat transfer coefficient. Heat reduction was computed using eq. (1) while considering the following: $\int_0^{l/2}(T_t-T_{t-\Delta t})\mathrm{d}l=S$, eq. (1) then becomes:

$$\varphi = c_p \rho AS. \quad (2)$$

Within $t-\Delta t$ to t seconds, the heat (φ) taken away by water flow on the surface equals the reduction of the plate and can be calculated as a function of the temperature difference between the surroundings and the surface:

$$\varphi = h_{t-\Delta t} A \int_{t-\Delta t}^{t} \left(T_f - T_w\right) \mathrm{d}t, \quad (3)$$

where $h_{t-\Delta t}$ denotes the surface heat transfer coefficient at $t-\Delta t$ moment. Then, we considered the following equation: $\int_{t-\Delta t}^{t} \left(T_f - T_w\right) \mathrm{d}t = P$, eq. (3) then becomes:

$$\varphi = h_{t-\Delta t} AP, \quad (4)$$

From eq. (2) and eq. (4), the surface heat-transfer coefficient at $t-\Delta t$ moment is given by the following:

$$h_{t-\Delta t} = \frac{c_p \rho S}{P}. \quad (5)$$

Eq. (5) shows that the heat transfer coefficient is proportional to heat reduction and inversely proportional to the temperature difference between the surface and the surroundings.

3.2.2 *Heat transfer coefficient with time*

Figure 5 shows the heat transfer coefficient for every second, as calculated by eq. (5). Corresponding to the above-mentioned cooling process, which can be divided into four steps, the coefficients followed a different trend. In the starting step, the coefficients were small. In the rapid cooling step, the coefficients increased significantly following a linear trend, and they increased with increasing quenching flux. In the slow cooling step, the coefficients increased slightly, and peaks appeared at the end of this step. In the stopping step, the coefficient decreased remarkably in a linear trend.

Figures 3–5 show that in the rapid cooling step, despite the highest surface cooling rate and heat flux observed, the coefficient was not the highest. However, in the slow cooling step, when the cooling rate decreased, the coefficient reached the peak. In the rapid cooling step, the surface temperature decreases gradually from a significantly high value, thus resulting in the reduction of the temperature difference between the surface and surroundings. The coefficient is inversely proportional to the temperature difference (see eq. (5)). Thus, despite the significantly high heat flux, the coefficient was small at the beginning and increased with the reduction in the temperature difference. However, the surface temperature has decreased remarkably to a considerably low value in the rapid cooling step. As a result, the surface temperature changed minimally in the following steps, and the same result was observed for temperature differences. Hence, although heat flux decreased, the coefficient reached the peak in the following slow cooling step.

3.2.3 *Effect of surface temperature and quenching flux*

According to the corresponding relationship between the surface temperature and time, the coefficient curve of time can be transferred to the surface temperature, as shown in Figure 6. Results showed that the coefficient increased with decreasing surface temperature. For example, in test L40, in the starting step (I), the coefficient gradually increased from a very low value to ~2500 W m^{-2} °C^{-1}, and the temperature ranged from 480 to 440°C. In the rapid cooling step (II), the coefficient increased from 2500 to 15000 W m^{-2} °C^{-1} with surface temperature ranging from 440 to 145°C. In the slow cooling step (III), the coefficient increased to a peak value of 20000 W m^{-2} °C^{-1}, with the temperature changing from 150 to 100°C. Finally, when completing step (IV), the coefficient decreased significantly below 100°C. L35 and L23 exhibited trends that were similar to that of L40. However, the coefficient decreased with the reduction of quenching flux. The trends of these curves agree with measurements obtained by Wang et al. [14].

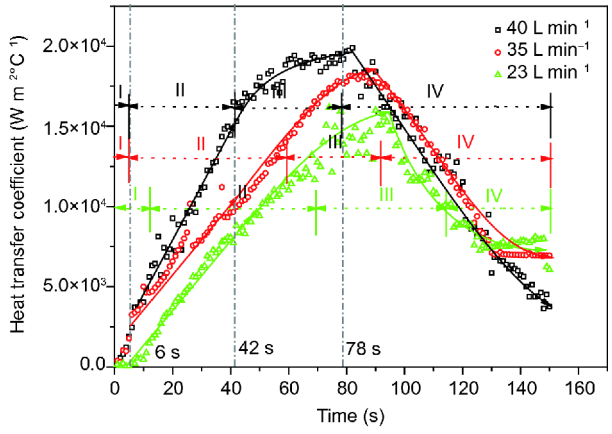

Figure 5 (Color online) Heat transfer coefficient at every second of different quenching flux, the cooling process was divided into the following four steps: (I) starting step, (II) rapid cooling step, (III) slow cooling step, and (IV) stopping step.

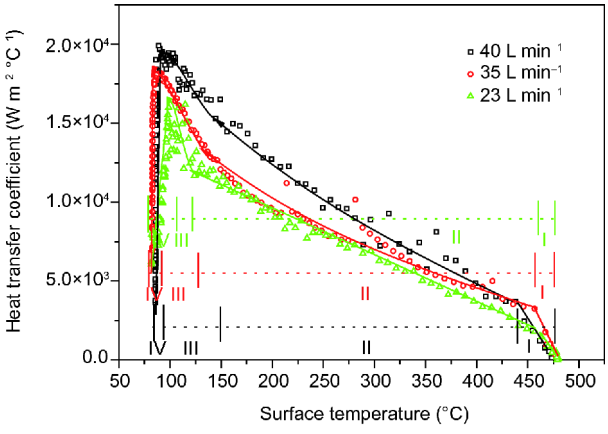

Figure 6 (Color online) Heat transfer coefficient at different surface temperatures, the cooling process is divided into the following four steps: (I) starting step, (II) rapid cooling step, (III) slow cooling step, and (IV) stopping step.

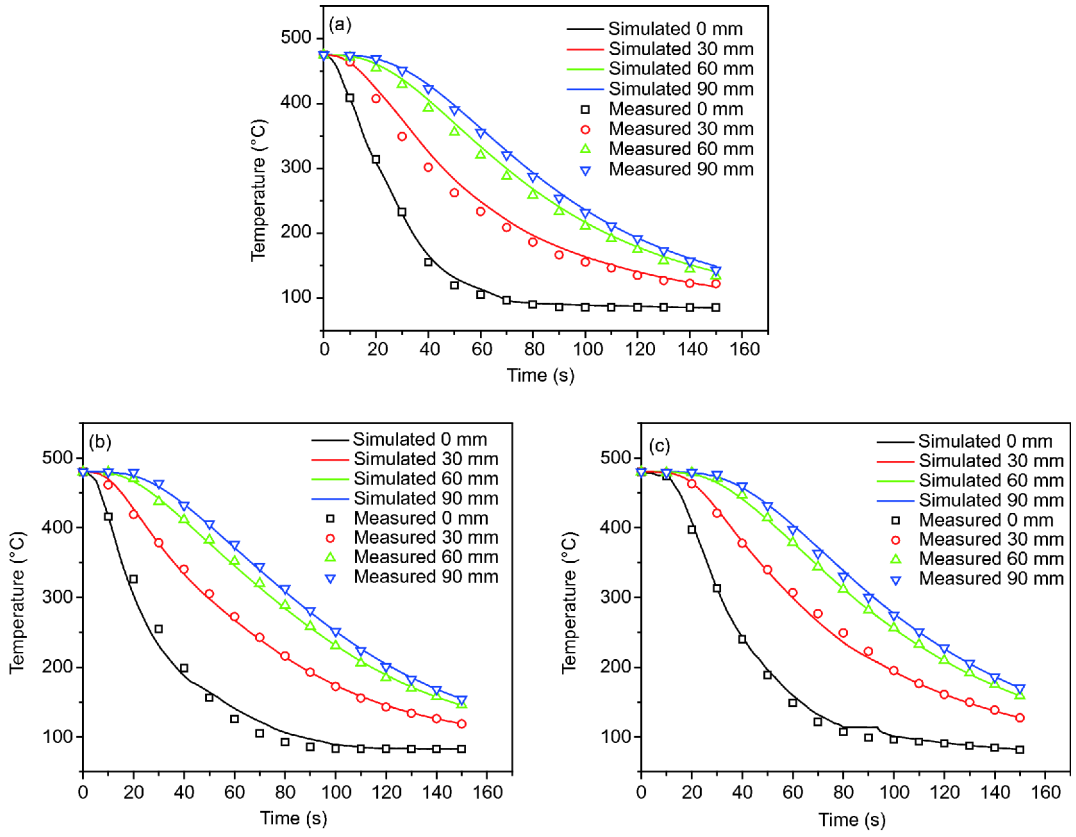

Figure 7 (Color online) Comparison of the simulated cooling curves with measurements, the flux of large flow area measured (a) 40, (b) 35, and (c) 23 L min^{-1}.

3.3 Verification by simulation

The temperature field of this quenching process was simulated using the finite element method software ABAQUS 6.10. The size of the geometry model was 0.018 m×0.11 m×0.13 m. Table 1 lists the thermal parameters used in simulation. The heat transfer coefficient used in this simulation was obtained by eq. (5), as shown in Figure 6. The model was meshed in the equal mesh method, and an element type of C3D8T was selected. To coordinate the actual conditions of temperature measurements, the coefficient was assigned only to the upper and lower surfaces and not to the side face of the plate. The initial plate temperature measured 480°C.

After the simulation, the cooling curves at the same locations were compared with actual measurements, and the results are shown in Figure 7. The simulation curves showed good agreement with the measurements, thus indicating the credibility of the heat transfer coefficient and the calculation method.

4 Conclusions

(1) In this investigation, based on the cooling curves and heat flux curves, the cooling process comprised the following four steps: (I) the starting step, (II) rapid cooling step, (III) slow cooling step, and (IV) stopping step. The highest heat transfer coefficient was observed not in the rapid cooling step with the largest heat flux but in the slow cooling step with the lower heat flux.

(2) The coefficient gradually increased with reduction in the surface temperature from 480 to 150°C. The coefficient peaked at temperatures ranging from 150 to 100°C with a sudden increase, but it decreased significantly below 100°C. The coefficient also increased with the quenching flux of large flow area in the rapid and slow cooling steps.

(3) The cooling curves by simulation showed good agreement with the measurements, thus verifying the accuracy of the heat transfer coefficient and calculation method.

This work was supported by the National Basic Research Program of China (Grant No. 2012CB619500), the Major State Research Program of China (Grant No. 2016YFB0300901), the National Natural Science Foundation of China (Grant No. 51375503) and the BaGui Scholars Program of China's Guangxi Zhuang Autonomous Region (Grant No. 2013A017).

1 Zhang X M, Deng Y L, Zhang Y. Development of high strength aluminum alloys and processing techniques for the materials. Acta Metall Sin, 2015, 51: 257–271
2 Rioja R J, Liu J. The evolution of Al-Li base products for aerospace and space applications. Metall Mat Trans A, 2012, 43: 3325–3337
3 Tang J, Chen H, Zhang X, et al. Influence of quench-induced pre-

cipitation on aging behavior of Al-Zn-Mg-Cu alloy. Trans Nonferr Met Soc China, 2012, 22: 1255–1263
4 Rossini N S, Dassisti M, Benyounis K Y, et al. Methods of measuring residual stresses in components. Mater Des, 2012, 35: 572–588
5 Liu W, He Z, Chen Y, et al. Dynamic mechanical properties and constitutive equations of 2519A aluminum alloy. Trans Nonferr Met Soc China, 2014, 24: 2179–2186
6 Wang W, Zhang X, Gao Z, et al. Influences of Ce addition on the microstructures and mechanical properties of 2519A aluminum alloy plate. J Alloys Compd, 2010, 491: 366–371
7 Robinson J S, Tanner D A, Truman C E, et al. The influence of quench sensitivity on residual stresses in the aluminium alloys 7010 and 7075. Mater Charact, 2012, 65: 73–85
8 Farahani S D, Kowsary F, Ashjaee M. Experimental investigation of heat transfer coefficient from the impingement of a slot jet using conjugate gradient method with adjoint equation. Exp Heat Trans, 2016, 29: 657–672
9 Sagheby S H, Kowsary F. Experimental design and methodology for estimation of local heat transfer coefficient in jet impingement using transient inverse heat conduction problem. Exp Heat Transfer, 2009, 22: 300–315
10 Gnanasekaran N, Balaji C. An inexpensive technique to simultaneously determine total emissivity and natural convection heat transfer coefficient from transient experiments. Exp Heat Transfer, 2010, 23: 235–258
11 Price R F, Fletcher A J. Determination of surface heat-transfer coefficients during quenching of steel plates. Met Tech, 1980, 7: 203–211
12 Wang M, Yang G, Huang C, et al. Simulation of temperature and stress in 6061 aluminum alloy during online quenching process. Trans Nonferr Met Soc China, 2014, 24: 2168–2173
13 Yang X, Zhu J, Lai Z, et al. Finite element analysis of quenching temperature field, residual stress and distortion in A357 aluminum alloy large complicated thin-wall workpieces. Trans Nonferr Met Soc China, 2013, 23: 1751–1760
14 Wang H, Yu W, Cai Q. Experimental study of heat transfer coefficient on hot steel plate during water jet impingement cooling. J Mater Proc Tech, 2012, 212: 1825–1831
15 Zhang J, Deng Y, Yang W, et al. Design of the multi-stage quenching process for 7050 aluminum alloy. Mater Des (1980–2015), 2014, 56: 334–344
16 Chen S, Chen K, Peng G, et al. Effect of quenching rate on microstructure and stress corrosion cracking of 7085 aluminum alloy. Trans Nonferr Met Soc China, 2012, 22: 47–52
17 Newkirk J W, MacKenzie D S. The Jominy end quench for lightweight alloy development. J Mater Eng Perform, 2000, 9: 408–415
18 Liu S, You J, Zhang X, et al. Influence of cooling rate after homogenization on the flow behavior of aluminum alloy 7050 under hot compression. Mater Sci Eng-A, 2010, 527: 1200–1205